

NNLO QCD CALCULATIONS WITH THE SECTOR-IMPROVED RESIDUE SUBTRACTION SCHEME*

RENE PONCELET

Cavendish Laboratory, Cambridge, United Kingdom

(Received April 28, 2020)

Precise predictions for total and differential cross sections at hadron colliders are at the heart of LHC physics. The lack of new ‘smoking-gun’ physics signals requires precise comparisons between measurements and Standard Model predictions to get a handle on New Physics effects. Tremendous efforts have been made to push perturbative calculations to higher orders such that NNLO QCD calculations are now state-of-the-art for most $2 \rightarrow 1$ and $2 \rightarrow 2$ hard scattering processes. Upcoming five-point two-loop amplitudes and refined subtractions schemes for real radiation contributions allow now first steps in the direction of $2 \rightarrow 3$ scattering processes.

DOI:10.5506/APhysPolB.51.1503

1. Introduction

Hadron colliders such as the LHC are considered to be discovery machines, probing a vast range of energies to unveil unknown physics in form of new interactions or Beyond Standard Model (BSM) particle content. However, this discovery potential comes with a trade-off, the hadronic environment in which hard scattering processes take place creates complex final states. The experimental analysis becomes very challenging and this increases the complexity of theoretical predictions. Any interaction, the Standard Model (SM) or BSM, is subject to important QCD corrections, and the theory community has to use the full portfolio of techniques to get theory uncertainties under control. The motivation for ever increasing theoretical precision and accuracy is not only a better understanding of the SM itself, but also the fact that no ‘smoking gun’ new physics signal has been observed in data yet. Precise comparisons between the SM and measurements will

* Presented at XXVI Cracow Epiphany Conference on LHC Physics: Standard Model and Beyond, Kraków, Poland, January 7–10, 2020.

allow for an indirect method to probe for New Physics. The quest for greater precision and accuracy has many aspects but fixed-order perturbative calculations form an essential part of any theory prediction. A tremendous progress in this field has been observed in the past decade, mainly driven by the introduction of new calculation techniques and better implementation of established methods. Next-to-leading order (NLO) QCD and NLO electro-weak corrections are widely automatised, matched to Monte Carlo programs, and used by experiments and theorists for the LHC physics modelling.

Predictions at next-to-next-to-leading order in perturbation theory become more and more available, in particular for QCD. State-of-the-art are low multiplicity (less than three final-state particles) SM processes. For the availability of higher multiplicity processes, two aspects are essential, the availability of two-loop amplitudes and the handling of the infra-red singularities in the double real-emission contributions. The computation of two-loop amplitudes is a challenging task and, so far, is done manually process by process. There are several attempts to automatise numerical computations, as has been done at one-loop [1–4], make progress, but they are still far from being fully general and applicable. The cutting edge are two-loop 5-point amplitudes, where planar results are already obtained [5, 6]. To deal with the real radiation contributions, various subtraction or slicing methods have been developed (corresponding literature can be found in [7]). The four-dimensional sector-improved residue subtraction scheme proposed in [8] has been applied successfully to different LHC processes. The implementation of the scheme into a flexible C++ framework, called *Stripper*, allows for an efficient workflow to implement new processes and observables. The first computation done with this framework was the differential cross sections for $t\bar{t}$ pair production [9]. To overcome inefficiencies in the way the subtraction phase space has been constructed, a new phase-space parameterization has been proposed in [7] and implemented. These changes allow to minimize the number of subtraction kinematics in each sector, resulting in a more efficient Monte Carlo integration, in particular for differential distributions. The new scheme has been recently applied to top-quark pair production and decay [10], inclusive jet production [7] and, additionally, it has been used to obtain the first NNLO QCD calculation of a $2 \rightarrow 3$ process, the production of three photons [6].

2. Top-quark pair production and decay in the Narrow-Width Approximation

The modelling of the top-quark decays enriches the phenomenology of top-quark pair production considerably. On the one hand, it allows to study features of quark pairs which are inaccessible in the case of a stable top-quark computation like spin-correlations and, on the other hand, it is possible to

study the impact of NNLO QCD corrections closer to experimental reality where the decay products rather than the on-shell top-quarks are measured. The **Stripper** framework has been modified to allow for heavy particle decays within the Narrow-Width Approximation (NWA), including full spin correlations. In particular, the di-leptonic top-quark decay channel has been implemented up to NNLO QCD [10]. The spin-correlation of the top-quark pair is a particular well-suited topic to be studied in such a computational setup. Conceptually, the spin density matrix [11] encodes all the information about polarization and correlations, but is difficult to access experimentally, since a reconstruction of the top-quark momenta is necessary and the spin-vectors are only known indirectly over the spin-analysing power of the decay products. However, some differential observables directly related to the decay products encode spin correlations between the top-quark parents. One example is the azimuthal opening angle $\Delta\phi_{\ell\bar{\ell}}$ of the two charged leptons. Experimentally, this observable is easily accessible and allows for more precise measurements since no top-quark reconstruction is necessary to study them in the experimental fiducial phase-space volume. Yet, fiducial phase-space definitions usually require a careful understanding of the phase-space cuts. The ATLAS study [12] discusses a measurement of this observable in the fiducial phase space and an extrapolation to the inclusive phase space. A tension in the shape of the $\Delta\phi_{\ell\bar{\ell}}$ differential cross section with respect to the NLO SM Monte Carlo predictions has been observed in the extrapolated phase-space volume. For this particular case, the NNLO QCD predictions for $\Delta\phi_{\ell\bar{\ell}}$ have been computed and presented in [10]. Details about the calculation are not reproduced here and are only summarized.

As it can be seen in Fig. 1, the NNLO QCD corrections loosen the tension in the inclusive phase space but do not resolve them completely. On the other hand, within the fiducial phase space, they are well-described by the NNLO predictions, see Fig. 2. In this context, an additional issue about the definition of normalized differential cross sections became clear. The shown differential cross sections are normalized to the full (inclusive or fiducial) cross section

$$R = \frac{1}{\sigma} \frac{d\sigma}{dX}.$$

To be explicit on how the normalized differential distributions in Figs. 1 and 2 have been obtained, we consider the following perturbative expansions:

$$\begin{aligned} \sigma &= \sigma^0 + \alpha_S \sigma^1 + \alpha_S^2 \sigma^2, \\ \frac{d\sigma}{dX} &= \frac{d\sigma^0}{dX} + \alpha_S \frac{d\sigma^1}{dX} + \alpha_S^2 \frac{d\sigma^2}{dX}, \end{aligned}$$

where X is a infra-red safe observable. The PDFs used for the computations are matched to the perturbative order, thus we compute

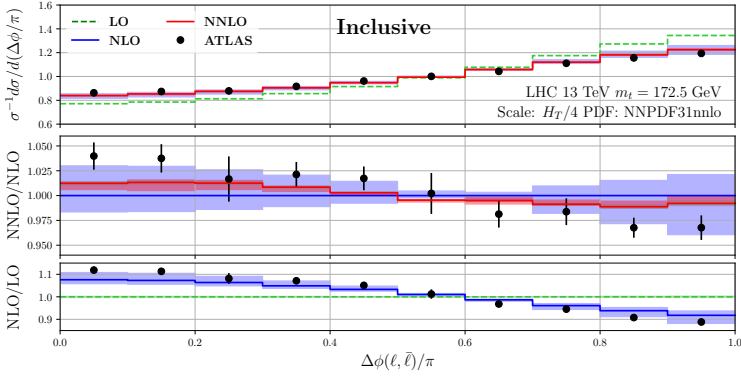


Fig. 1. Normalized differential cross section with respect to $\Delta\phi_{\ell\bar{\ell}}$ within the inclusive phase space as described in [10].

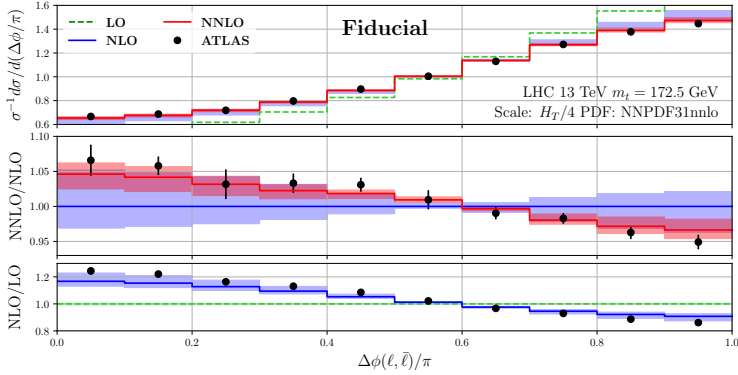


Fig. 2. Normalized differential cross section with respect to $\Delta\phi_{\ell\bar{\ell}}$ within the fiducial phase space as described in [10].

$$\begin{aligned}\sigma^{\text{LO}} &= \sigma^0 \quad \text{with } \sigma^i \text{ computed with LO PDFs,} \\ \sigma^{\text{NLO}} &= \sigma^0 + \alpha_S \sigma^1 \quad \text{with } \sigma^i \text{ computed with NLO PDFs,} \\ \sigma^{\text{NNLO}} &= \sigma^0 + \alpha_S \sigma^1 + \alpha_S^2 \sigma^2 \quad \text{with } \sigma^i \text{ computed with NNLO PDFs,}\end{aligned}$$

and similar for the differential ones. We thus obtain the normalized differential cross section at NNLO by defining

$$R^{\text{NNLO}} = \frac{1}{\sigma^{\text{NNLO}}} \frac{d\sigma^{\text{NNLO}}}{dX},$$

and similar for the lower orders. If we consider the normalization, we see that $1/\sigma$ might be re-expanded in α_S such that one obtains a series expansion for R

$$\begin{aligned}
 R &= \frac{1}{\sigma} \frac{d\sigma}{dX} = R^0 + \alpha_S R^1 + \alpha_S^2 R^2, \\
 R^0 &= \frac{1}{\sigma^0} \frac{d\sigma^0}{dX}, \\
 R^1 &= \frac{1}{\sigma^0} \frac{d\sigma^1}{dX} - \frac{\sigma^1}{\sigma^0} \frac{1}{\sigma^0} \frac{d\sigma^0}{dX}, \\
 R^2 &= \frac{1}{\sigma^0} \frac{d\sigma^2}{dX} - \frac{\sigma^1}{\sigma^0} \frac{1}{\sigma^0} \frac{d\sigma^1}{dX} + \left(\left(\frac{\sigma^1}{\sigma^0} \right)^2 - \frac{\sigma^2}{\sigma^0} \right) \frac{1}{\sigma^0} \frac{d\sigma^0}{dX}.
 \end{aligned}$$

To again specify the used PDFs, we evaluate analogously

$$\begin{aligned}
 R^{\text{LO,exp}} &= R^0 \quad \text{with } \sigma^i \text{ computed with LO PDFs,} \\
 R^{\text{NLO,exp}} &= R^0 + \alpha_S R^1 \quad \text{with } \sigma^i \text{ computed with NLO PDFs,} \\
 R^{\text{NNLO,exp}} &= R^0 + \alpha_S R^1 + \alpha_S^2 R^2 \quad \text{with } \sigma^i \text{ computed with NNLO PDFs.}
 \end{aligned}$$

When considering scale variations, the scale is varied everywhere simultaneously, in the numerator as well the denominator. In Fig. 3, we show the differences between the expanded and not expanded normalized differential

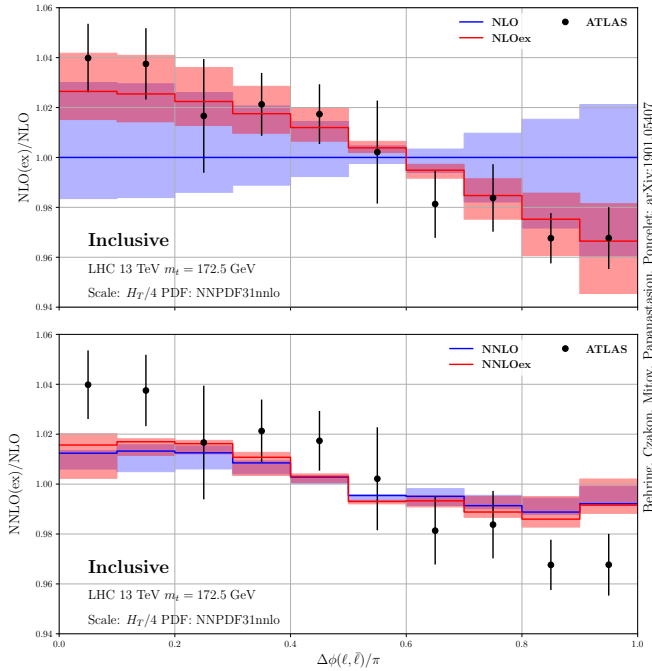


Fig. 3. Expanded normalized differential cross section with respect to $\Delta\phi_{\ell\bar{\ell}}$ within the inclusive phase space as described in [10].

cross section. In particular, one can observe that at NLO, while being consistent within scale uncertainty, the shape of the $\Delta\phi_{\ell\bar{\ell}}$ distribution changes significantly when expanding the cross section. However, this ambiguous behaviour is resolved at NNLO, where both methods give consistent results. It cannot be stressed enough that the NNLO predictions significantly improves the scale dependence, in both definitions of the normalized differential cross section.

3. Inclusive jet cross sections with full colour dependence

The production of jets is naturally the most common hard scattering process at hadron colliders. It is phenomenologically interesting due to the sensitivity to QCD parameters such as PDFs, α_S or new physics at high-energy scales. Inclusive jet rates have been considered to be good benchmark, for PDF determination and allow to pin-point large- x gluon PDFs. They are

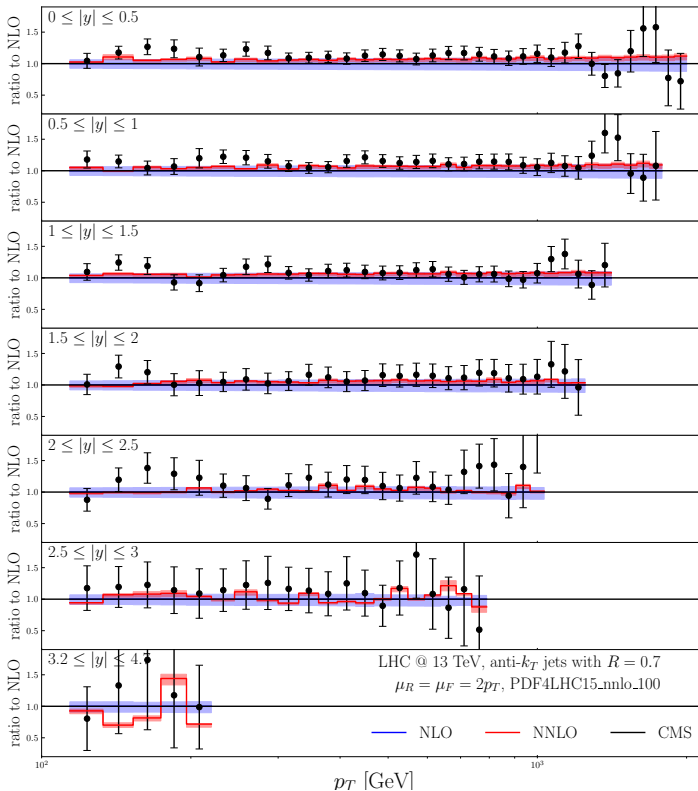


Fig. 4. Single inclusive jet rates in bins of jet transverse momentum and pseudorapidity, details on the setups can be found in [13].

also interesting from the perturbative QCD point of view as the underlying partonic processes exhibit all possible QCD limits at NNLO. This makes this process particularly difficult to compute, but by the same token might serve as benchmark for computation schemes. Double differential inclusive jet rates at NNLO QCD have been obtained by the NNLOJet Collaboration, for example [13] within the leading colour approximation for the fermionic contributions. The first computation with full colour dependence has been obtained in [7]. The inclusive jet rates in bins of the jet transverse momentum p_T and pseudo-rapidity $|\eta|$ are shown in Fig. 4. The NNLO QCD prediction shows reduced scale dependence and reasonable K-factors with respect to NLO ranging from 1 to 10% and general good agreement with CMS data. A comparison with the results from the NNLOJet Collaboration shows that there is no significant difference due to the sub-leading colour effects and thus those effects can be estimated to be less than 1% which corresponding to statistical uncertainty from the Monte Carlo integration in the most precise bins.

4. Three photon production

A natural next step is to go to higher multiplicity processes *e.g.*, with genuine $2 \rightarrow 3$ kinematics. The main bottleneck here is the availability of two-loop virtual matrix elements. A lot of progress has been made in the past few years to tackle the easiest class of $2 \rightarrow 3$ processes, those with all external and internal particles massless. Different approaches are in development to achieve an efficient evaluation of the relevant matrix elements. Numerical reconstruction methods have been successfully applied to achieve analytic expressions for all planar (leading colour) pure QCD helicity amplitudes in the Euclidean phase-space region [13]. The first (planar) $2 \rightarrow 3$ amplitude in the physical region has been computed in [6] for the three photon production process $q\bar{q} \rightarrow \gamma\gamma\gamma$. The approach has made use of the known analytic IBP reductions for the planar topologies [14] and a representation of the planar master integrals in terms of iterated integrals [15]. Non-planar contributions to the full matrix elements are not yet available due to the lack of IBP relations and an appropriate representation of the master integrals. The master integrals have been derived only in terms of differential equations and numerical boundary conditions suitable for numerical evaluations [16]. Thus, a representation of the non-planar amplitude in terms of a function basis is not feasible yet. For an NNLO QCD computation, the relevant $q\bar{q} \rightarrow \gamma\gamma\gamma$ matrix element can be decomposed in the following way:

$$\begin{aligned} \overline{\sum} 2\text{Re} \langle M^{(2)} | M^{(0)} \rangle &= M^{(\text{lc}, 1)} (N_c^3 - 2N_c + 1/N_c) + M^{(\text{lc}, 2)} (N_c^3 - N_c) \\ &\quad + M^{(f)} (N_c^2 - 1) + M^{(\text{np})} (N_c - 1/N_c) . \end{aligned}$$

The $M^{(\text{lc},1)}$ ($M^{(\text{lc},2)}$) parts contain all planar diagrams with non-Abelian (no non-Abelian) couplings. The $M^{(f)}$ features all planar diagrams with fermion loops while $M^{(\text{np})}$ collects all non-planar diagrams. The computation of the non-planar part $M^{(\text{np})}$ is not yet within reach and thus, since it also contains fermion loop diagrams, it is not possible to include the $M^{(f)}$ contributions consistently due to gauge invariance. We then obtain the gauge-invariant planar part of the amplitude by neglecting everything but $M^{(\text{lc},1)}$ and $M^{(\text{lc},1)}$. The series in the dimensional regularization parameter ϵ of the matrix element is computed in a straightforward manner in terms of the ‘pentagon’-function basis

$$\overline{\sum} 2\text{Re} \left\langle M^{(2)} | M^{(0)} \right\rangle (\vec{x}) = \sum_{i=-4}^0 \sum_{k \in \mathcal{F}_i} \epsilon^i f^k(\vec{x}) c_{ik}(\vec{x}),$$

where $f^k(\vec{x})$ is a short-hand for the various pentagon functions (and corresponding products) and \mathcal{F}_i represents the set of functions that appear at a given order in ϵ . The rational coefficients $c_{ik}(\vec{x})$ are implemented after simplification using rational numbers to avoid loss of precision in intermediate steps. They are simplified by using **Fermat** and **Mathematica**. For the most complicated coefficients, rational field reconstruction as implemented in the **FiniteFlow** [17] software is used to add up the large amount of individual terms. The pentagon functions are evaluated with the public available code from [15]. The final implementation needs 10 to 50 mins for a single evaluation of the full matrix element. This is mostly due to the large set of functions appearing in the final result. The evaluation of the two-loop finite remainder function from the matrix element is the computationally most expensive part in this NNLO QCD computation. We evaluated 30 000 phase-space points from unweighted tree-level events. The computation of the other NNLO QCD contribution, real–virtual and double real corrections, has been computed within the **Stripper** framework and has been computationally cheap (roughly 2000 CPU hours). All one-loop matrix elements have been obtained from the **OpenLoops** [18] software.

A phenomenological study of the production of three isolated photons at NNLO QCD has been performed for the experimental setup of [19]. For details about phase-space cuts and other parameters I refer the interested reader to [6]. A central observable is the fiducial cross section within the phase-space constraints, and the perturbative QCD results are shown in Fig. 5.

The NNLO QCD corrections are significant and improve the agreement with the ATLAS measurement which is only poorly described by NLO QCD. The corrections are far outside of the theory uncertainty estimates from scale variation at lower order, which has already been observed in various

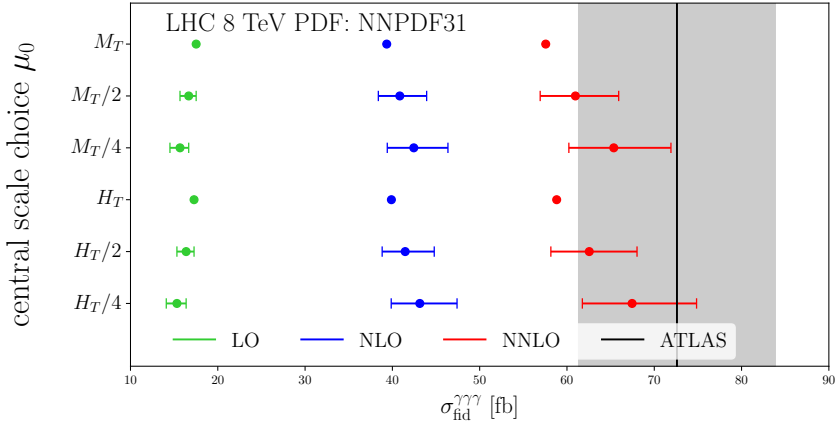


Fig. 5. Fiducial cross sections from perturbative QCD for the production of three isolated photons compared to ATLAS measurement [19].

colour singlet production processes. A very close example is the photon-pair production [20], which shows very similar features. Differentially, a selection of observables can be found in Fig. 6. We observe a significant improvement in the description of the ATLAS measurement in terms of normalization and also non-trivial shapes. As already pointed out, the large NNLO/NLO K-factors are very similar to those observed for the two-photon process. However, there is a particular difference between two and three photons which is the absence of a gg -box contribution in the latter. The

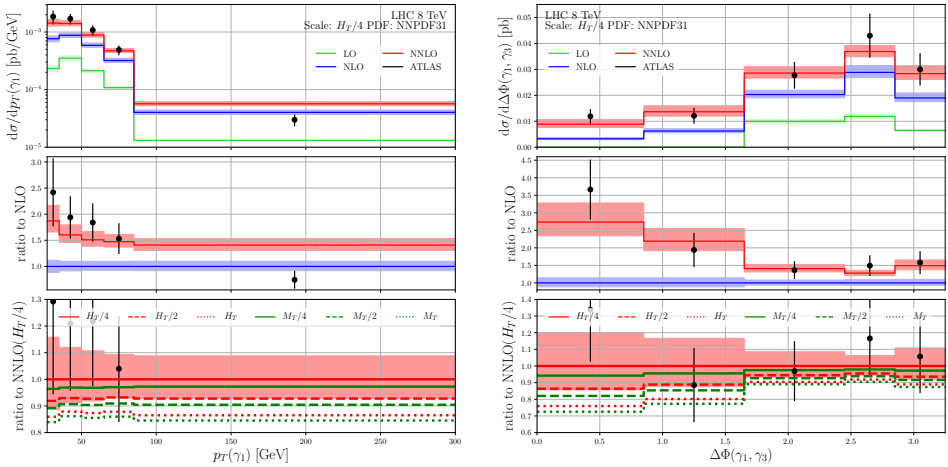


Fig. 6. Differential cross section with respect to the leading photon $p_T(\gamma_1)$ (left) and the azimuthal opening angle $\Delta\Phi(\gamma_1, \gamma_2)$ compared against ATLAS measurements.

corresponding one-loop amplitudes for the $gg \rightarrow \gamma\gamma\gamma$ process vanish due to Furry's theorem. As pointed out in [20], analogous contributions in the photon pair process give a +10% contribution to the cross section. For the three-photon process, the gg initial state only enters through the double real radiation contribution at NNLO. In Fig. 7, the cross section is decomposed in the different partonic fluxes as computed from LHAPDF for the used NNPDF3.1 PDF set. Here, the gg channel gives only a small contribution to the total cross section. At the next order (N^3 LO), the gg channel would also contribute through a separately finite loop-induced contribution from the process $gg \rightarrow \gamma\gamma\gamma g$. The contribution of this higher order correction is estimated to be very small.

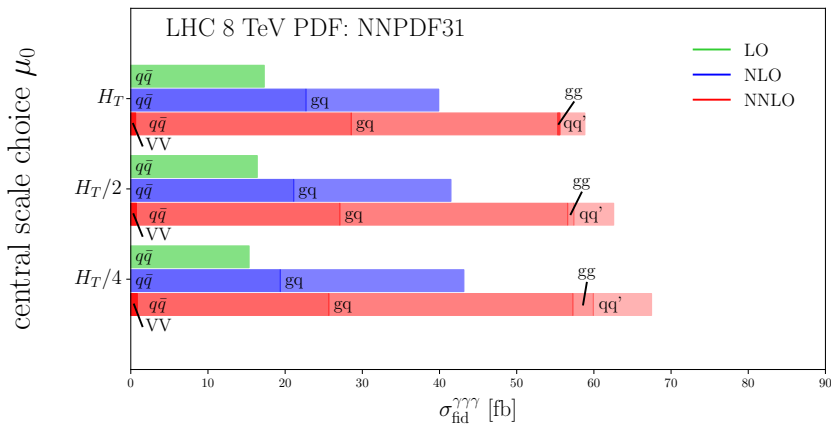


Fig. 7. Decomposition of the fiducial cross section for three-photon production into partonic fluxes.

5. Summary and outlook

Precision predictions for LHC processes are important and will gain importance while more and more precise measurements from Run 2 and the future high-luminosity phase appear. Great efforts are made to improve theoretical predictions in accuracy and precision. Fixed-order perturbation theory is an important tool to understand the SM and has been pushed forward to higher orders and more complicated final states. The state-of-the-art for low multiplicity processes is now NNLO QCD, possibly supplemented with NLO EW. The two main difficulties are subtraction methods and computations of virtual matrix elements. NNLO QCD subtraction methods are on their way to be generally applicable and automated. The calculations presented in this letter demonstrate the current capabilities of the **Stripper** framework as a flexible and automated scheme. The phenomenological applications furthermore demonstrate important implication of NNLO QCD

corrections, from strongly reduced scale uncertainties in top-quark pair and jet observables to large K-factors like in the production of three photons. The latter process is also the first ever $2 \rightarrow 3$ process computed at NNLO QCD and opens up a new chapter in NNLO QCD perturbative calculations. The methods to obtain the (planar) two-loop matrix elements are generic and can be applied to other massless $2 \rightarrow 3$ processes, opening up more possibilities for phenomenological studies at NNLO QCD.

The research of R.P. has received funding from the European Research Council (ERC) under the European Union's Horizon 2020 research and innovation programme (grant agreement No. 683211).

REFERENCES

- [1] F. Cascioli, P. Maierhofer, S. Pozzorini, *Phys. Rev. Lett.* **108**, 111601 (2012), [arXiv:1111.5206 \[hep-ph\]](#).
- [2] S. Actis *et al.*, *Comput. Phys. Commun.* **214**, 140 (2017), [arXiv:1605.01090 \[hep-ph\]](#).
- [3] V. Hirschi *et al.*, *J. High Energy Phys.* **1105**, 044 (2011), [arXiv:1103.0621 \[hep-ph\]](#).
- [4] G. Cullen *et al.*, *Eur. Phys. J. C* **72**, 1889 (2012), [arXiv:1111.2034 \[hep-ph\]](#).
- [5] S. Abreu *et al.*, *J. High Energy Phys.* **2019**, 084 (2019), [arXiv:1904.00945 \[hep-ph\]](#).
- [6] H.A. Chawdhry, M.L. Czakon, A. Mitov, R. Poncelet, *J. High Energy Phys.* **2020**, 057 (2020), [arXiv:1911.00479 \[hep-ph\]](#).
- [7] M. Czakon, A. van Hameren, A. Mitov, R. Poncelet, *J. High Energy Phys.* **2019**, 262 (2019), [arXiv:1907.12911 \[hep-ph\]](#).
- [8] M. Czakon, D. Heymes, *Nucl. Phys. B* **890**, 152 (2014), [arXiv:1408.2500 \[hep-ph\]](#).
- [9] M. Czakon, D. Heymes, A. Mitov, *Phys. Rev. Lett.* **116**, 082003 (2016), [arXiv:1511.00549 \[hep-ph\]](#).
- [10] A. Behring *et al.*, *Phys. Rev. Lett.* **123**, 082001 (2019), [arXiv:1901.05407 \[hep-ph\]](#).
- [11] W. Bernreuther, A. Brandenburg, *Phys. Rev. D* **49**, 4481 (1994), [arXiv:hep-ph/9312210](#).
- [12] ATLAS Collaboration (M. Aaboud *et al.*), [arXiv:1903.07570 \[hep-ex\]](#).
- [13] J. Currie *et al.*, *J. High Energy Phys.* **2018**, 155 (2018), [arXiv:1807.03692 \[hep-ph\]](#).
- [14] H.A. Chawdhry, M.A. Lim, A. Mitov, *Phys. Rev. D* **99**, 076011 (2019), [arXiv:1805.09182 \[hep-ph\]](#).

- [15] T. Gehrmann, J. Henn, N. Lo Presti, *J. High Energy Phys.* **2018**, 103 (2018), [arXiv:1807.09812](#) [[hep-ph](#)].
- [16] D. Chicherin *et al.*, *Phys. Rev. Lett.* **123**, 041603 (2019), [arXiv:1812.11160](#) [[hep-ph](#)].
- [17] T. Peraro, *J. High Energy Phys.* **2019**, 031 (2019), [arXiv:1905.08019](#) [[hep-ph](#)].
- [18] F. Buccioni *et al.*, *Eur. Phys. J. C* **79**, 866 (2019), [arXiv:1907.13071](#) [[hep-ph](#)].
- [19] ATLAS Collaboration (M. Aaboud *et al.*), *Phys. Lett. B* **781**, 55 (2018), [arXiv:1712.07291](#) [[hep-ex](#)].
- [20] J.M. Campbell, R.K. Ellis, C. Williams, *Phys. Rev. Lett.* **118**, 222001 (2017), [arXiv:1612.04333](#) [[hep-ph](#)].